

From angle-action to Cartesian coordinates: A key transformation for molecular dynamics

M. L. González-Martínez*

*Departamento de Física General, Instituto Superior de Tecnologías y Ciencias Aplicadas, Habana 6163, Cuba and
Institut des Sciences Moléculaires, Université Bordeaux 1,
351 Cours de la Libération, 33405 Talence Cedex, France*

L. Bonnet,[†] P. Larrégaray, and J. -C. Rayez
*Institut des Sciences Moléculaires, Université Bordeaux 1,
351 Cours de la Libération, 33405 Talence Cedex, France*

J. Rubayo-Soneira

Departamento de Física General, Instituto Superior de Tecnologías y Ciencias Aplicadas, Habana 6163, Cuba
(Dated: October 31, 2018)

The transformation from angle-action variables to Cartesian coordinates is a crucial step of the (semi) classical description of bimolecular collisions and photo-fragmentations. The basic reason is that dynamical conditions corresponding to experiments are ideally generated in angle-action variables whereas the classical equations of motion are ideally solved in Cartesian coordinates by standard numerical approaches. To our knowledge, the previous transformation is available in the literature only for triatomic systems. The goal of the present work is to derive it for polyatomic ones.

I. INTRODUCTION

Molecular reaction dynamics studies aim at understanding chemical reactions and inelastic collisions at the atomic scale. In other words, this field of research draws much of the conceptual framework in which chemical reactivity, in a broad sense, can be thought [1].

Quantum state-resolved integral and differential cross sections (ICSs and DCSs), measured in supersonic molecular beam experiments, are among the most fundamental observables of molecular reaction dynamics. This paper deals with their classical mechanical description in a semi-classical spirit.

Most processes considered up to now involve three or four atoms, on purpose. This allows both measurements at an amazing level of detail and accurate theoretical descriptions of the observables from first principles. Additionally, planetary atmospheres and interstellar clouds are mainly made of small species which dynamics should be understood.

Nowadays, however, much of molecular science is polarized on larger systems, like nano-objects or molecules of biological interest, and the natural trend in molecular reaction dynamics is also to move towards increasing complexity. More and more polyatomic processes are thus under scrutiny.

State-of-the-art descriptions of state-resolved ICSs and DCSs are in principle performed within the framework of exact quantum scattering approaches (EQS) [2, 3, 4, 5, 6, 7, 8, 9]. However, despite the impressive progress

of computer performance achieved in the last decades, these approaches can hardly be applied to larger than three or four-atom systems as the basis sizes necessary for converging the calculations turn prohibitive.

A popular alternative is the quasi-classical trajectory method (QCTM) [10, 11, 12]. This approach is intuitive, relatively easy to implement, much less time consuming than EQS approaches and therefore, quite appealing for studying polyatomic processes. The price to pay is obviously a loss in accuracy as compared to EQS approaches. Nevertheless, significant advances have been made in the last few years through the replacement of the standard binning (SB) procedure by the Gaussian weighting (GW) one [13, 14, 15, 16, 17, 18, 19]. In the SB method, each trajectory has the same statistical weight. On the other hand, the GW procedure consists in weighting each trajectory by a Gaussian-like coefficient such that the closer the final actions to integer values, the larger the coefficient. This procedure proves to be especially efficient when few vibrational levels are available in the final products. Though initially proposed on the basis of rather intuitive arguments, the GW procedure can be shown to find its roots in classical S matrix theory, the former semi-classical approach of molecular collisions pioneered by Miller and Marcus in the early seventies [20, 21, 22].

Central quantities of chemical reaction theory are (1) the state-to-state reaction probabilities P_{mn} , where \mathbf{n} and \mathbf{m} are reagent and product quantum states, (2) the densities $dP_{mn}/d\theta$, where θ is the scattering angle or any given angle of the problem and (3) the capture probabilities $P_{\mathbf{n}}$ for processes involving long-lived intermediate complexes [23]. From these quantities, any state-resolved ICS and DCS can be determined.

To calculate the previous probabilities (or density of), one must generate classical dynamical conditions corre-

*Corresponding author, E-mail: mleo@instec.cu

[†]Corresponding author, E-mail: l.bonnet@ism.u-bordeaux1.fr

sponding to quantum state n . Such a generation is readily performed in angle-action coordinates [20, 22, 24] as these are in close correspondence with quantum numbers. On the other hand, angle-action variables should not be used to run trajectories as contrary to Cartesian coordinates, they lead to strong numerical instabilities. The transformation from angle-action variables to Cartesian coordinates is therefore a crucial step of QCTM.

For atom-diatom (semi) collisions, this transformation can be found in the book by Whittaker [25] and in a paper by Miller [26]. However, we have not been able to find in the literature the analogous transformation for a generic type of collision. The goal of the paper is to thus to derive it.

II. THEORY

In this work, a prototype system is presented, namely a five-atom molecule made of a triatomic (ABC) and a diatomic (DE). The former can be used as a model for a non-linear polyatomic fragment while the latter constitutes a simpler case very commonly found in practice. The transformation provided here will therefore be relevant for a generic pair of molecular fragments, *e.g.* diatom + diatom, asymmetric top + diatom, asymmetric top + asymmetric top, etc... after straightforward generalizations. These, along with the transformations in [25, 26] allow thus to treat any case of interest.

We suppose the fragments are to be studied in the low energy regime where only the lowest vibrational states can be populated, thus the harmonic description of their vibrations is a reasonably accurate approximation. Anharmonic corrections can be introduced when necessary.

Throughout this work, the usual convention of bold-facing vector magnitudes is used. Cartesian frames centered on a generic point P are represented as (P, x, y, z) . A given vector \mathbf{a} in such a frame will be rewritten as \mathbf{a}' if we refer it to (P, x', y', z') instead. Calligraphic letters are used for representing matrices and second-rank tensors. Some standard transformations, *e.g.* that of normal modes to Cartesian coordinates, are included for completeness. Finally, the two fragments, ABC and DE, are numbered 1 and 2 and so are their associated magnitudes.

A. Cartesian coordinates

The system is schematically represented in Fig. 1. Three Cartesian frames of reference are used: (1) the laboratory frame which origin is at the molecular center of mass G and is in uniform translation so that the total center-of-mass movement can be effectively removed, and (2, 3) the two body-fixed, non-inertial reference frames with origins at each fragment's center of mass, denoted G_1 and G_2 . The Cartesian coordinates to which transformation from angle-actions is made are defined as the

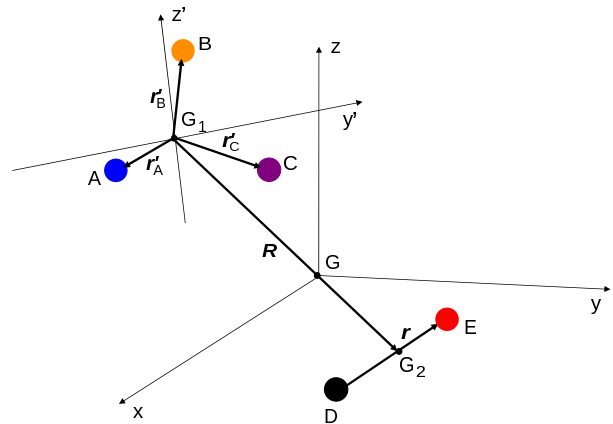


FIG. 1: A prototypical five-atom system represented in its center-of-mass reference frame. A triatomic and diatomic potential fragments are outlined.

complete set of nuclei positions \mathbf{R}_X , in the (G, x, y, z) space, plus their conjugate momenta \mathbf{P}_X , with $X \in \{A, B, \dots, E\}$. The total number of such coordinates yields, of course, $6 \times 5 = 30$.

B. Angle-action coordinates

Of the 30 variables chosen, 8 are not angle-actions, *i.e.* (1, 2) the distance R between the fragments centers of mass G_1 and G_2 and its conjugate momentum P [34]; and (3-8) the position and momentum vectors for the molecular center of mass, G. The 22 angle-action variables are thus:

q_i : the vibrational phase of the i th normal mode of ABC, $i = \overline{1, 3}$.

$\hbar x_i$: the vibrational action of the i th normal mode of ABC, $i = \overline{1, 3}$.

q_4 : the vibrational phase of DE.

$\hbar x_4$: the vibrational action of DE.

J : the modulus of the total angular momentum \mathbf{J} .

α : the angle conjugate to \mathbf{J} .

J_z : the algebraic value of the projection of \mathbf{J} on the laboratory z axis.

β : the angle conjugate to J_z .

l : the modulus of the orbital angular momentum \mathbf{l} .

α_l : the angle conjugate to l .

j_1 : the modulus of the rotational angular momentum \mathbf{j}_1 of ABC.

- α_1 : the angle conjugate to j_1 .
- j_2 : the modulus of the rotational angular momentum \mathbf{j}_2 of DE.
- α_2 : the angle conjugate to j_2 .
- k : the modulus of the total rotational angular momentum $\mathbf{k} = \mathbf{j}_1 + \mathbf{j}_2$.
- α_k : the angle conjugate to k .
- κ_1 : the algebraic value of the projection of \mathbf{j}_1 on one of the three axes of inertia of ABC.
- γ_1 : the angle conjugate to κ_1 .

The six triatomic normal mode coordinates fully specify the three position vectors $\mathbf{r}'_A = (y'_A, z'_A)$, $\mathbf{r}'_B = (y'_B, z'_B)$ and $\mathbf{r}'_C = (y'_C, z'_C)$, in the (y', z') plane of the body-fixed (G_1, x', y', z') frame of ABC. z' is arbitrarily made to coincide with one of the ABC axes of inertia when it happens to be in its equilibrium geometry. These six normal mode coordinates also define the three momentum vectors $\mathbf{p}'_A = (p_{Ay'}, p_{Az'})$, $\mathbf{p}'_B = (p_{By'}, p_{Bz'})$ and $\mathbf{p}'_C = (p_{Cy'}, p_{Cz'})$, conjugate to the three previous position vectors, *i.e.* 12 coordinates as a whole. Note that these twelve Cartesian coordinates are deduced from the six normal modes plus six constraints due to the fact that ABC is neither in translation nor in rotation in the (G_1, y', z') plane.

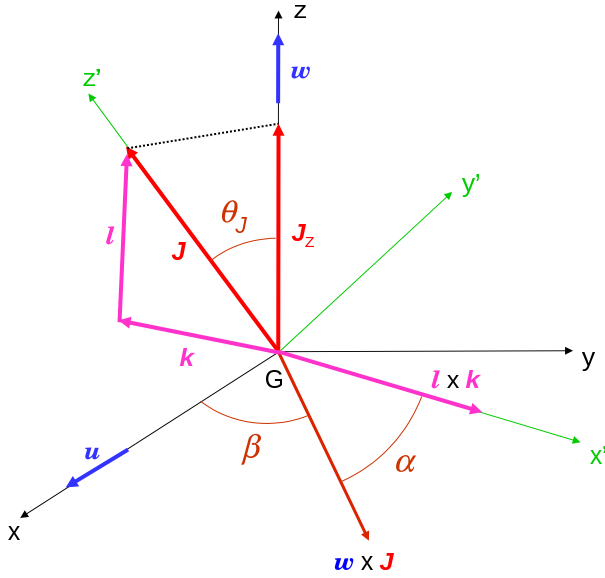


FIG. 2: Some angular momentum vectors and angles.

The total angular momentum \mathbf{J} , its z -component J_z , their conjugate angles α and β as well as the orbital \mathbf{l} and total rotational \mathbf{k} angular momenta are represented in Fig. 2. The unit vectors along the x and z axes are respectively denoted \mathbf{u} and \mathbf{w} . We wish to emphasize here that the three axes x' , y' and z' used at this point

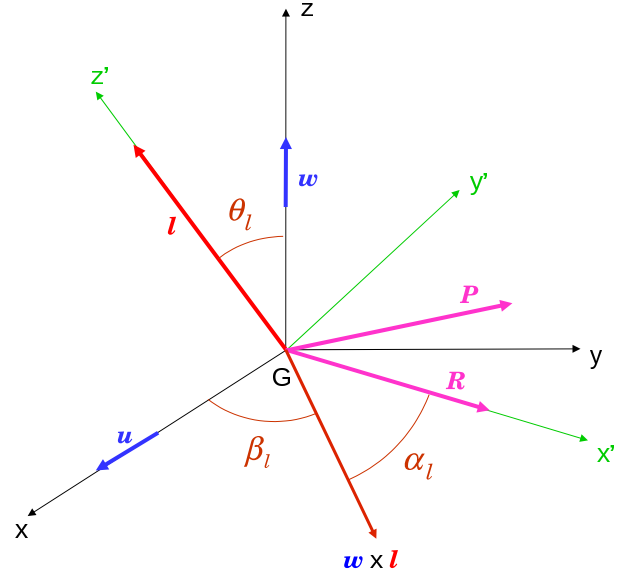


FIG. 3: Spatial relation among the total orbital angular momentum \mathbf{l} , the intermolecular Jacobi vector \mathbf{R} and its conjugate momentum \mathbf{P} .

have nothing to do with the primed axes introduced in the previous paragraph. Several primed frames will be defined in the following which will be different from each other. β is the angle between \mathbf{u} and $\mathbf{w} \times \mathbf{J}$ while α is the angle between $\mathbf{w} \times \mathbf{J}$ and $\mathbf{l} \times \mathbf{k}$.

\mathbf{l} is represented in Fig. 3 together with the Jacobi vector \mathbf{R} between G_1 and G_2 . α_l is the angle between $\mathbf{w} \times \mathbf{l}$ and \mathbf{R} . The momentum \mathbf{P} conjugate to \mathbf{R} is also depicted. Like \mathbf{R} , \mathbf{P} lies in the plane orthogonal to \mathbf{l} .

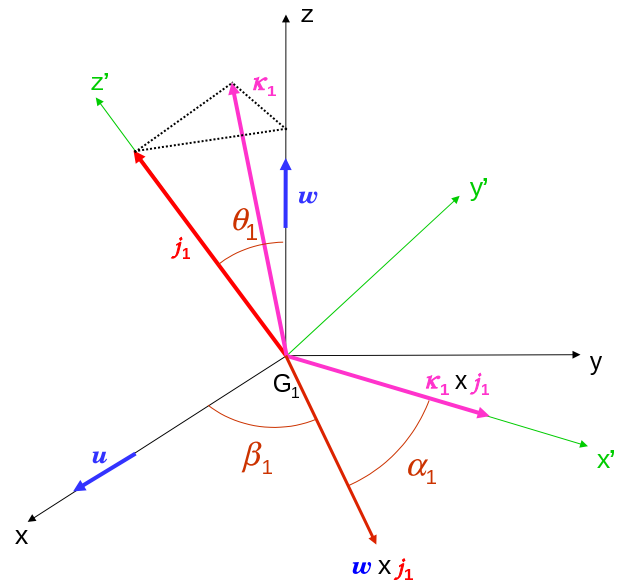


FIG. 4: ABC angular momentum vectors and some angles.

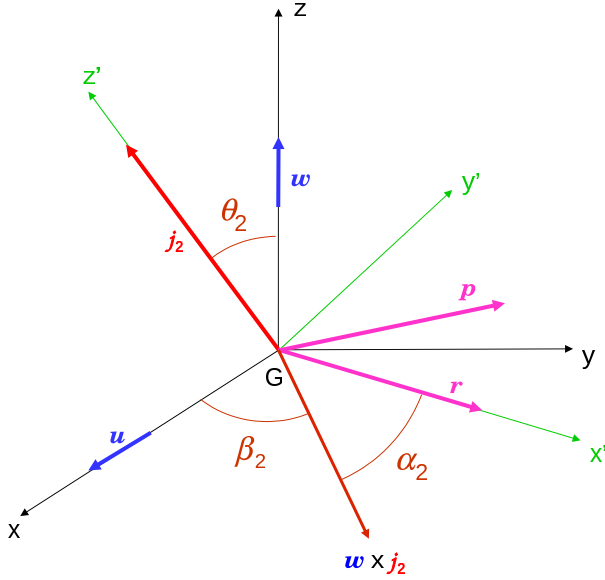


FIG. 5: Spatial relation among the diatomic rotational angular momentum j_2 , the DE interatomic Jacobi vector r and its conjugate momentum p .

j_1 is represented in Fig. 4 together with κ_1 , defined as the projection of j_1 on the z' axis of the previously specified body-fixed frame of ABC. α_1 is the angle between $w \times j_1$ and $\kappa_1 \times j_1$.

j_2 is represented in Fig. 5 together with the Jacobi vector r between the D and E atoms. α_2 is the angle between $w \times j_2$ and r . The momentum p conjugate to r is also represented. Both r and p lie in the plane orthogonal to j_2 .

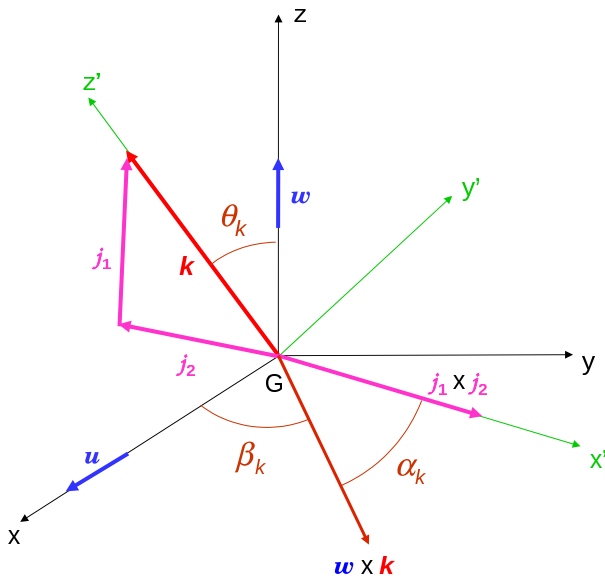


FIG. 6: Some angular momentum vectors and angles.

The link between k , j_1 and j_2 is isomorphic to the one between J , l and k , as easily seen from the comparison between Fig. 6 and Fig. 2. α_k is thus the angle between $w \times k$ and $j_1 \times j_2$. Calling w' the unit vector along the z' axis of the ABC body-fixed frame, the algebraic value κ_1 equals plus (minus) $|\kappa_1|$ when w' and j_1 make an angle lower (larger) than $\pi/2$. Finally, γ_1 is the angle between $w \times \kappa_1$ and the x' axis in Fig. 4.

C. Transformation from angle-action to Cartesian coordinates

The algorithm for computing initial conditions from the title transformation will vary slightly according to the specific application (*e.g.* unimolecular dissociation, bimolecular collision...) and/or the experimental conditions to be reflected. The transformations, however, are intrinsically general so we assume in what follows that all angle-action variables, as well as R and P , are either known or can be computed by the time they are referred to during the process. The transformation can be decomposed in 11 steps, each making the subject of one of the following sections. It is important to note that the ordering given here is somewhat arbitrary and need for reordering may arise in specific applications.

1. Cartesian components of l .

In Fig. 7, the vectors J , l and k are represented in the plane (G, y', z') as deduced from Fig. 2. The relation between these angular momenta can be written as

$$J - l = k. \quad (2.1)$$

Squaring each side of the previous equality and rearranging leads to

$$\cos \theta_{Jl} = \frac{J^2 + l^2 - k^2}{2Jl}. \quad (2.2)$$

l'_z , equal to $l \cos \theta_{Jl}$, is thus given by

$$l'_z = \frac{J^2 + l^2 - k^2}{2J}. \quad (2.3)$$

l'_y , equal to $l \sin \theta_{Jl}$, *i.e.*, to $l(1 - \cos^2 \theta_{Jl})^{1/2}$ (given the convention adopted, l'_y is necessarily positive), is therefore given by

$$l'_y = \left[l^2 - \left(\frac{J^2 + l^2 - k^2}{2J} \right)^2 \right]^{1/2}. \quad (2.4)$$

At last, l'_x is zero.

l is deduced from l' by the standard Euler rotation

$$l = \mathcal{M}_3(-\beta)\mathcal{M}_1(-\theta_J)\mathcal{M}_3(-\alpha)l', \quad (2.5)$$

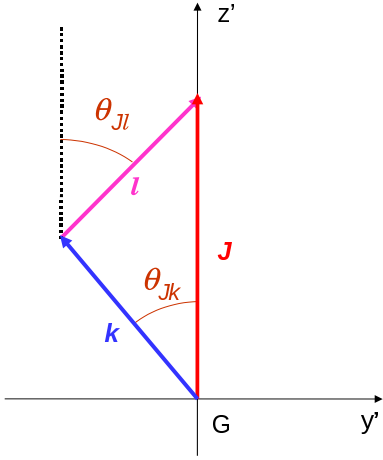


FIG. 7: Spatial relation between the total \mathbf{J} , orbital \mathbf{l} and rotational \mathbf{k} angular momenta.

where, for a given angle χ ,

$$\mathcal{M}_1(-\chi) = \begin{pmatrix} 1 & 0 & 0 \\ 0 & \cos \chi & -\sin \chi \\ 0 & \sin \chi & \cos \chi \end{pmatrix} \quad (2.6)$$

and

$$\mathcal{M}_3(-\chi) = \begin{pmatrix} \cos \chi & -\sin \chi & 0 \\ \sin \chi & \cos \chi & 0 \\ 0 & 0 & 1 \end{pmatrix}. \quad (2.7)$$

Indeed, Fig. 2 shows that one goes from (G, x', y', z') to (G, x, y, z) by a rotation of $-\alpha$ around the z' axis followed by a rotation of $-\theta_J$ around the resulting, ‘new’ x' axis and a final rotation of $-\beta$ around the ‘new’ z' axis. One may easily check that these transformations are achieved by the \mathcal{M}_1 and \mathcal{M}_3 matrices combined as in Eq. 2.5.

$\cos \theta_J$ is given by

$$\cos \theta_J = \frac{J_z}{J} \quad (2.8)$$

and $\sin \theta_J$, necessarily positive as $\theta_J \in [0, \pi]$, is given by

$$\sin \theta_J = \left[1 - \left(\frac{J_z}{J} \right)^2 \right]^{1/2}. \quad (2.9)$$

2. Cartesian components of \mathbf{R} .

From Fig. 3 and following the same reasoning as above, \mathbf{R} can be shown to satisfy

$$\mathbf{R} = \mathcal{M}_3(-\beta_l) \mathcal{M}_1(-\theta_l) \mathcal{M}_3(-\alpha_l) \mathbf{R}', \quad (2.10)$$

where \mathbf{R}' represents the vector $(R, 0, 0)$. Fig. 8 shows how the angles β_l and θ_l relate to \mathbf{l} . $\cos \theta_l$ is given by

$$\cos \theta_l = \frac{l_z}{l} \quad (2.11)$$

and $\sin \theta_l$, necessarily positive, by

$$\sin \theta_l = \left[1 - \left(\frac{l_z}{l} \right)^2 \right]^{1/2}. \quad (2.12)$$

$\cos \beta_l$ is given by

$$\cos \beta_l = -\frac{l_y}{l_{xy}} \quad (2.13)$$

and $\sin \beta_l$ by

$$\sin \beta_l = \frac{l_x}{l_{xy}}, \quad (2.14)$$

where

$$l_{xy} = (l^2 - l_z^2)^{1/2} \quad (2.15)$$

is the modulus of the projection of \mathbf{l} on the (G, x, y) plane, as depicted in Fig. 8.

3. Cartesian components of \mathbf{P} .

Since $\mathbf{l} = \mathbf{R} \times \mathbf{P}$, \mathbf{P} lies in the plane (G, x', y') of Fig. 3, P'_x has already been denoted P , P'_y equals l/R and P'_z is zero. \mathbf{P} is then obtained with

$$\mathbf{P} = \mathcal{M}_3(-\beta_l) \mathcal{M}_1(-\theta_l) \mathcal{M}_3(-\alpha_l) \mathbf{P}'. \quad (2.16)$$

4. Cartesian components of \mathbf{k} .

We still consider Fig. 7 and rewrite the relation between \mathbf{J} , \mathbf{l} and \mathbf{k} as

$$\mathbf{J} - \mathbf{k} = \mathbf{l}. \quad (2.17)$$

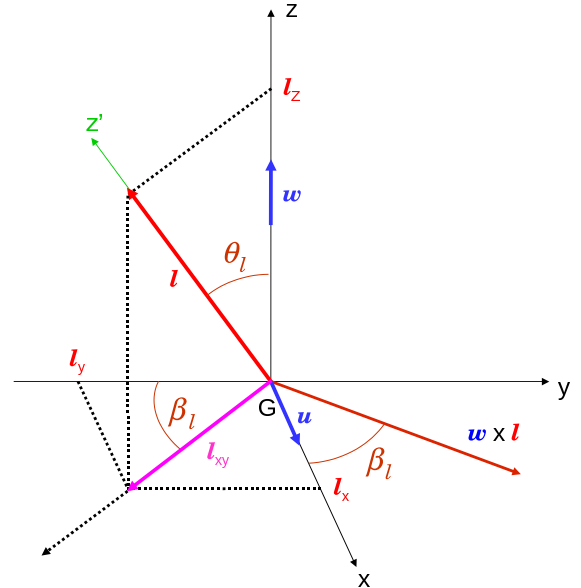


FIG. 8: Orbital angular momentum \mathbf{l} , its Cartesian components and conjugate angles.

Squaring each side of the previous equality and rearranging leads to

$$\cos \theta_{Jk} = \frac{J^2 + k^2 - l^2}{2Jk}. \quad (2.18)$$

k'_z , equal to $k \cos \theta_{Jk}$, is thus given by

$$k'_z = \frac{J^2 + k^2 - l^2}{2J}. \quad (2.19)$$

k'_y , equal to $-k \sin \theta_{Jk}$, *i.e.*, to $-k(1 - \cos^2 \theta_{Jk})^{1/2}$ (given the convention adopted, k'_y is necessarily negative), is therefore given by

$$k'_y = - \left[k^2 - \left(\frac{J^2 + k^2 - l^2}{2J} \right)^2 \right]^{1/2} \quad (2.20)$$

(one may check that k'_y is the just the opposite of l'_y). At last, k'_x is zero. \mathbf{k} is then obtained from \mathbf{k}' by the same transformation that relates \mathbf{l} to \mathbf{l}' (see Eq. 2.5)

$$\mathbf{k} = \mathcal{M}_3(-\beta) \mathcal{M}_1(-\theta_J) \mathcal{M}_3(-\alpha) \mathbf{k}'. \quad (2.21)$$

5. Cartesian components of \mathbf{j}_1 and \mathbf{j}_2 .

As already seen, the determination of \mathbf{j}_1 and \mathbf{j}_2 is in complete analogy with that of \mathbf{l} and \mathbf{k} (compare Fig. 6 and Fig. 2). Following the developments in sections II C 1 and II C 4, we then arrive at

$$\mathbf{j}_i = \mathcal{M}_3(-\beta_k) \mathcal{M}_1(-\theta_k) \mathcal{M}_3(-\alpha_k) \mathbf{j}'_i, \quad i = 1, 2; \quad (2.22)$$

where $j'_{1x} = j'_{2x} = 0$,

$$j'_{1y} = \left[j_1^2 - \left(\frac{k^2 + j_1^2 - j_2^2}{2k} \right)^2 \right]^{1/2}, \quad (2.23)$$

$$j'_{1z} = \frac{k^2 + j_1^2 - j_2^2}{2k}, \quad (2.24)$$

$$j'_{2y} = -j'_{1y} \quad (2.25)$$

and

$$j'_{2z} = \frac{k^2 + j_2^2 - j_1^2}{2k}. \quad (2.26)$$

In addition, $\cos \theta_k$ is given by

$$\cos \theta_k = \frac{k_z}{k} \quad (2.27)$$

and $\sin \theta_k$ by

$$\sin \theta_k = \left[1 - \left(\frac{k_z}{k} \right)^2 \right]^{1/2}. \quad (2.28)$$

$\cos \beta_k$ is given by

$$\cos \beta_k = -\frac{k_y}{k_{xy}} \quad (2.29)$$

and $\sin \beta_k$ by

$$\sin \beta_k = \frac{k_x}{k_{xy}}, \quad (2.30)$$

where

$$k_{xy} = (k^2 - k_z^2)^{1/2} \quad (2.31)$$

is the modulus of the projection of \mathbf{k} on the (G, x, y) plane.

6. Cartesian components of \mathbf{r} .

In the harmonic limit, the DE bond length r is given in terms of q_4 and $\hbar x_4$ by the expression

$$r = r_{\text{eq}} + \left[\frac{(2x_4 + 1)\hbar}{\mu_2 w_2} \right]^{1/2} \sin q_4. \quad (2.32)$$

Here, r_{eq} is the equilibrium bond length of the diatomic, μ_2 its reduced mass and w_2 its vibrational frequency (which is readily determined from a quadratic fitting of its interaction potential). Although x_4 is sometimes called action, *stricto sensu*, this is only true in \hbar units.

The problem of the determination of \mathbf{r} is then analogous to that of \mathbf{R} . From Fig. 5 and following section II C 2, we find

$$\mathbf{r} = \mathcal{M}_3(-\beta_2) \mathcal{M}_1(-\theta_2) \mathcal{M}_3(-\alpha_2) \mathbf{r}', \quad (2.33)$$

where \mathbf{r}' represents the vector $(r, 0, 0)$. $\cos \theta_2$ is given by

$$\cos \theta_2 = \frac{j_{2z}}{j_2} \quad (2.34)$$

and $\sin \theta_2$ by

$$\sin \theta_2 = \left[1 - \left(\frac{j_{2z}}{j_2} \right)^2 \right]^{1/2}. \quad (2.35)$$

$\cos \beta_2$ is given by

$$\cos \beta_2 = -\frac{j_{2y}}{j_{2xy}} \quad (2.36)$$

and $\sin \beta_2$ by

$$\sin \beta_2 = \frac{j_{2x}}{j_{2xy}}, \quad (2.37)$$

where

$$j_{2xy} = (j_2^2 - j_{2z}^2)^{1/2} \quad (2.38)$$

is the modulus of the projection of \mathbf{j}_2 on the (G, x, y) plane.

7. Cartesian components of \mathbf{p} .

Again, the problem of the determination of \mathbf{p} is analogous to that of the determination of \mathbf{P} . Following section II C 3, we arrive at

$$\mathbf{p} = \mathcal{M}_3(-\beta_2)\mathcal{M}_1(-\theta_2)\mathcal{M}_3(-\alpha_2)\mathbf{p}', \quad (2.39)$$

where $\mathbf{p}' = (p, j_2/r, 0)$ and

$$p = [(2x_4 + 1)\hbar w_2 \mu_2]^{1/2} \cos q_4 \quad (2.40)$$

in the harmonic approximation.

8. Cartesian components of $\boldsymbol{\kappa}_1$.

\mathbf{j}_1 and $\boldsymbol{\kappa}_1$ are represented in Fig. 4 and Fig. 9. The coordinates of $\boldsymbol{\kappa}_1$ in (G_1, x', y', z') are given by $\kappa'_{1x} = 0$,

$$\kappa'_{1y} = |\kappa_1| \left[1 - \left(\frac{\kappa_1}{j_1} \right)^2 \right]^{1/2} \quad (2.41)$$

and

$$\kappa'_{1z} = \frac{\kappa_1^2}{j_1} \quad (2.42)$$

(the last equation comes from the fact that the cosine of the angle between $\boldsymbol{\kappa}_1$ and \mathbf{j}_1 is equal both to κ'_{1z}/κ_1 and κ_1/j_1 , as is obvious from Fig. 9). Proceeding as previously, we find

$$\boldsymbol{\kappa}_1 = \mathcal{M}_3(-\beta_1)\mathcal{M}_1(-\theta_1)\mathcal{M}_3(-\alpha_1)\boldsymbol{\kappa}'_1. \quad (2.43)$$

$\cos \theta_1$ is given by

$$\cos \theta_1 = \frac{j_{1z}}{j_1} \quad (2.44)$$

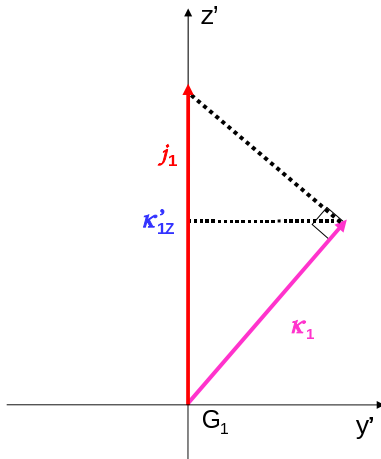


FIG. 9: Spatial relation between the triatomic rotational \mathbf{j}_1 and inertial-axis component $\boldsymbol{\kappa}_1$ angular momenta.

and $\sin \theta_1$ by

$$\sin \theta_1 = \left[1 - \left(\frac{j_{1z}}{j_1} \right)^2 \right]^{1/2}. \quad (2.45)$$

$\cos \beta_1$ is given by

$$\cos \beta_1 = -\frac{j_{1y}}{j_{1xy}} \quad (2.46)$$

and $\sin \beta_1$ by

$$\sin \beta_1 = \frac{j_{1x}}{j_{1xy}}, \quad (2.47)$$

where

$$j_{1xy} = (j_1^2 - j_{1z}^2)^{1/2} \quad (2.48)$$

is the modulus of the projection of \mathbf{j}_1 on the (G_1, x, y) plane.

9. Cartesian components of \mathbf{r}_A , \mathbf{r}_B and \mathbf{r}_C .

We start by determining the position vectors \mathbf{r}'_X for $X = A, B$ or C in the (G_1, x', y', z') frame (Fig. 1). Within the harmonic approximation, this task is accomplished by the standard normal mode analysis [12] (a generalization of the procedure used in the diatomic case; compare this and the following with sections II C 6 and II C 7).

First, the eigenvalues λ_i and eigenvectors \mathcal{L}_i of the Hessian matrix \mathcal{H} are determined. For an N -atom molecule, six of the former correspond to the center-of-mass movement and overall rotation and thus are theoretically zero (negligibly small in practice). The $3N - 6$ non-zero eigenvalues, associated with the molecule internal vibrational modes, relate to their angular frequencies simply by $w_i = \lambda_i^{1/2}$. Quasi-classical normal mode energies are then computed from the corresponding vibrational actions as

$$E_i = \hbar w_i \left(x_i + \frac{1}{2} \right), \quad (2.49)$$

which allows the calculation of the normal mode displacements

$$Q_i = \sqrt{\frac{2E_i}{\lambda_i}} \sin q_i. \quad (2.50)$$

Cartesian mass-weighted displacements are determined with $\boldsymbol{\eta} = \mathcal{L}\mathbf{Q}$, where \mathcal{L} is the eigenvector matrix and \mathbf{Q} that of normal mode coordinates. The position vectors \mathbf{r}'_X are thus

$$\mathbf{r}'_X = \mathbf{r}'_{X\text{eq}} + m_X^{-\frac{1}{2}} \boldsymbol{\eta}_X, \quad (2.51)$$

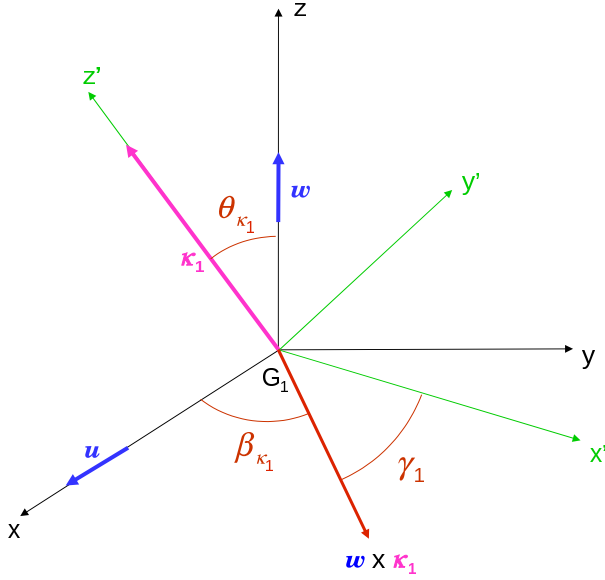


FIG. 10: Angular momentum vector κ_1 and some angles.

where $\mathbf{r}'_{X\text{eq}}$ are the equilibrium position vectors, m_X is the mass of atom X and $\boldsymbol{\eta}_X$ is extracted from $\boldsymbol{\eta}$ according to the location given to the X-atom coordinates in \mathcal{H} .

From Fig. 10, we have

$$\mathbf{r}_X = \frac{\kappa_1}{|\kappa_1|} \mathcal{M}_3(-\beta_{\kappa_1}) \mathcal{M}_1(-\theta_{\kappa_1}) \mathcal{M}_3(-\gamma_1) \mathbf{r}'_X, \quad (2.52)$$

which holds for X = A, B or C.

When κ_1 is positive, the (G_1, x', y', z') frames in Fig. 10 and Fig. 1 exactly coincide. Therefore, the dependence of \mathbf{r}_X on \mathbf{r}'_X is of the same kind as in the previous sections. If, on the other hand, κ_1 is negative, (G_1, x', y', z') in Fig. 10 is different from its equivalent in Fig. 1. In fact, in this case the y' and z' axes are oriented in the exact opposite directions as in the previous one. The term $\kappa_1/|\kappa_1|$, which equals -1 , takes this difference into account by flipping the vector $\mathcal{M}_3(-\beta_{\kappa_1}) \mathcal{M}_1(-\theta_{\kappa_1}) \mathcal{M}_3(-\gamma_1) \mathbf{r}'_X$ before it is identified as \mathbf{r}_X .

In Eq. 2.52, $\cos \theta_{\kappa_1}$ is given by

$$\cos \theta_{\kappa_1} = \frac{\kappa_{1z}}{|\kappa_1|} \quad (2.53)$$

and $\sin \theta_{\kappa_1}$ by

$$\sin \theta_{\kappa_1} = \left[1 - \left(\frac{\kappa_{1z}}{\kappa_1} \right)^2 \right]^{1/2}. \quad (2.54)$$

$\cos \beta_{\kappa_1}$ is given by

$$\cos \beta_{\kappa_1} = -\frac{\kappa_{1y}}{\kappa_{1xy}} \quad (2.55)$$

and $\sin \beta_{\kappa_1}$ by

$$\sin \beta_{\kappa_1} = \frac{\kappa_{1x}}{\kappa_{1xy}}, \quad (2.56)$$

where

$$\kappa_{1xy} = (\kappa_1^2 - \kappa_{1z}^2)^{1/2} \quad (2.57)$$

is, as usual, the modulus of the projection of κ_1 on the (G_1, x, y) plane.

10. Cartesian components of \mathbf{p}_A , \mathbf{p}_B and \mathbf{p}_C .

The momenta \mathbf{p}_X , with X = A, B or C, can be decomposed into a *purely* translational (vibrational) and a rotational components. Based on the very definition of the body-fixed (G_1, x, y, z) frame (Fig. 1), the former is directly related to \mathbf{p}'_X . To calculate these, normal-mode velocities are first computed using the conservation of energy

$$\dot{Q}_i = \pm(2E_i - \lambda_i Q_i^2)^{1/2}, \quad (2.58)$$

the sign being selected according to the value of the vibrational phase q_i . Cartesian mass-weighted velocities are thus $\dot{\boldsymbol{\eta}} = \mathcal{L}\dot{\mathbf{Q}}$ from which

$$\mathbf{p}'_X = m_X^{\frac{1}{2}} \dot{\boldsymbol{\eta}}_X. \quad (2.59)$$

It is important to stress that the anharmonicity of the real potential energy has been deliberately neglected within the normal-mode approximation. To correct for its possible spurious consequences, relatively sophisticated recipes can be used at this stage. The reader is thus referred to the available literature, *e.g.* [12], as it is not our objective to reproduce them here.

The rotational component is determined in the standard fashion. The triatomic angular velocity is computed as $\boldsymbol{\omega}_1 = \mathcal{I}^{-1} \mathbf{j}_1$ —being \mathcal{I} the inertia tensor of ABC, which can be calculated at this point since its configuration has been determined—from which, the corresponding linear velocities are given by

$$\boldsymbol{\nu}_X = \boldsymbol{\omega}_1 \times \mathbf{r}'_X. \quad (2.60)$$

Finally, the transformation relating \mathbf{p}_X and \mathbf{p}'_X is isomorphic to Eq. 2.52, so the desired general expression for computing the former reads

$$\mathbf{p}_X = \frac{\kappa_1}{|\kappa_1|} \mathcal{M}_3(-\beta_{\kappa_1}) \mathcal{M}_1(-\theta_{\kappa_1}) \mathcal{M}_3(-\gamma_1) \mathbf{p}'_X + m_X \boldsymbol{\nu}_X. \quad (2.61)$$

11. Nuclear positions and momenta in (G, x, y, z) .

At this point it is a simple task to finally express all Cartesian vectors in the laboratory frame. For X = A, B or C, \mathbf{R}_X is given by the general expression

$$\mathbf{R}_X = -\frac{M_2}{M_{\text{tot}}} \mathbf{R} + \mathbf{r}_X, \quad (2.62)$$

while if $X = D$ or E ,

$$\mathbf{R}_X = \frac{M_1}{M_{\text{tot}}} \mathbf{R} + \mathbf{r}_X. \quad (2.63)$$

In these equations, M_i stands for the mass of fragment i and M_{tot} is the system total mass.

Similar relations hold for the Cartesian momenta. For $X = A, B$ or C , these are computed using the general expression

$$\mathbf{P}_X = -\frac{m_X}{M_1} \mathbf{P} + \mathbf{p}_X. \quad (2.64)$$

At last, the diatomic momenta are given by

$$\mathbf{P}_D = \frac{m_D}{M_2} \mathbf{P} - \mathbf{p} \quad (2.65)$$

and

$$\mathbf{P}_E = \frac{m_E}{M_2} \mathbf{P} + \mathbf{p}. \quad (2.66)$$

III. KETENE UNIMOLECULAR DISSOCIATION: A TEST CASE.

The photo-fragmentation of ketene (CH_2CO) has been intensively investigated for over two decades, both experimental and theoretically (*e.g.* [27, 28, 29, 30, 31, 32]). Following photo-excitation to the \tilde{A}^1A'' states, the molecule undergoes either intersystem crossing or fast internal conversion to the low lying triplet and singlet electronic states. From these, dissociation into methylene and carbon monoxide occurs. Despite the triplet threshold lies $\sim 3150 \text{ cm}^{-1}$ below the singlet, the fact that it presents a small barrier to dissociation—of a few cents of inverse centimeters—makes the singlet channel statistically dominant from excess energies as low as $\sim 100\text{--}200 \text{ cm}^{-1}$. Such conditions make the system an effective prototype for a *barrierless polyatomic* unimolecular reaction on a *single* potential energy surface (PES).

In direct correspondence with the model transformation we introduced above, the molecule constitutes a five-atom system which dissociates into a triatomic and diatomic fragments. Additionally, the experimental excitations are compatible with the harmonic—normal mode—approximation for the CH_2 and CO products. In what follows we briefly report on the application of the title transformation to the study of this process. Full details and results will be given in a separate work so we simply introduce it here as a corroboratory test case.

In Fig. 11 we compare our calculations with the most recent experimental results [32] for the products translational energy distributions, in correlation with the rotational state of CO . A 308 nm laser is used in the experiment, corresponding to an excess energy of 2350 cm^{-1} . The theoretical results are obtained using the so-called *exit-channel corrected phase-space theory*, proposed by

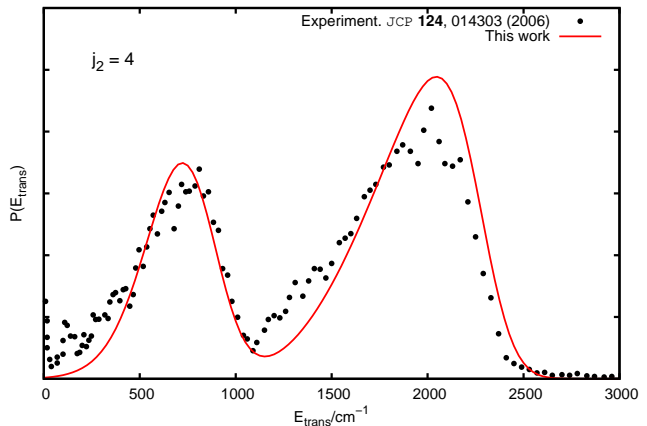


FIG. 11: Translational energy distribution in correlation with $j_2 = 4$, after excitation with a 308 nm laser. Comparison with the experiment.

Hamilton and Brumer [33]. This method basically consist in generating microcanonical initial conditions *at the products* and then propagate the trajectories backwards in time, the statistics being performed with those reaching the inner transition state (TS). The photo-excited ketene molecule is supposed to be long lived prior to its fragmentation, thereby justifying the use of a microcanonical distribution. We employed the high-level *ab initio* PES and transition state locations recently reported [30].

The theoretical predictions are in very good agreement with the experiment, as can be seen in Fig. 11. The curve has been artificially smoothed by using a convolution with an ‘apparatus’ function, *i.e.*

$$P(E_{\text{trans}}) = \int P(E') e^{-\beta(E' - E_{\text{trans}})^2} dE' \quad (3.67)$$

to recover the experimental tails. The two peaks correlating with the $v_2 = 0$ and $v_2 = 1$ CH_2 scissor-mode states are fairly well reproduced.

In order to further verify the validity of the transformation provided, we have calculated the determinant of the Jacobian matrix. The original is not a square matrix, with dimensions 30×24 . Therefore, for being able to calculate the determinant we introduced an additional transformation to a set of Jacobi coordinates, from which the (null) center-of-mass coordinates and momenta are later removed. The calculation starts with the transformation from angle-actions to Cartesian and from these to Jacobi coordinates. The center-of-mass Jacobi vectors are then removed and the determinant of the resulting 24×24 Jacobian matrix, from angle-actions to (reduced) Jacobi coordinates, is computed. We confirmed that it yields 1 within numerical accuracy.

IV. SUMMARY AND CONCLUSIONS

We have presented the transformation from angle-action to Cartesian coordinates, for polyatomic systems. In the quasi and semi-classical approaches, this provides an expeditious way to generate initial conditions in close correspondence with nowadays experiments and yet, solve the equations of motion using the ‘ideal’ Cartesian coordinates. The methodology and expressions provided here can either be directly used or straightforwardly generalized to deal with any case of interest, ranging from the study of bimolecular collisions to polyatomic unimolecular dissociations.

Preliminary results of the particular application to the study of the unimolecular dissociation of ketene in the singlet electronic state, have been discussed. A very

good agreement is observed between the experimental values and theoretical predictions for correlated translational energy distributions. The validity of the transformation have been further verified by numerical computation of the determinant of the Jacobian matrix, which yields unity within reasonable accuracy.

ACKNOWLEDGMENTS

Support from an Inter-University Agreement on International Joint Doctorate Supervision between the Instituto Superior de Tecnologías y Ciencias Aplicadas, Cuba and the Université Bordeaux 1, France, as well as the PNPAP/7/3 project of the Cuban institution, are gratefully acknowledged.

-
- [1] R. D. Levine, *Molecular Reaction Dynamics*, Cambridge University Press, Cambridge, 2005.
- [2] G. Nyman and H. G. Yu, *Rep. Prog. Phys.*, 2000, **63**, 1001.
- [3] P. Honvault and J. M. Launay in *Theory of Chemical Reaction Dynamics*; Kluwer Academic Publishers, 2004; p. 187.
- [4] V. Aquilanti and S. Tonzani, *J. Chem. Phys.*, 2004, **120**, 4066.
- [5] S. Althorpe in *The Encyclopedia of Computational Chemistry*, ed. P. v. R. Schleyer; Wiley InterScience, Athens, 2005.
- [6] W. Hu and G. C. Schatz, *J. Chem. Phys.*, 2006, **125**, 132301.
- [7] B. Lepetit, D. Wang, and A. Kuppermann, *J. Chem. Phys.*, 2006, **125**, 133505.
- [8] X. Q. Zhang, Q. Cui, J. Z. H. Zhang, and K. L. Han, *J. Chem. Phys.*, 2007, **126**, 234304.
- [9] D. D. Fazio, V. Aquilanti, S. Cavalli, A. Aguilar, and J. M. Lucas, *J. Chem. Phys.*, 2008, **129**, 064303.
- [10] R. N. Porter and L. M. Raff in *Dynamics of Molecular Collisions, Part B*, ed. W. H. Miller; Plenum, New York, 1976.
- [11] D. G. Truhlar and J. T. Muckerman, Plenum Press, New York, 1979; chapter Reactive Scattering Cross Sections: Quasiclassical and Semiclassical Methods, p. 505.
- [12] T. D. Sewell and D. L. Thompson, *Int. J. Mod. Phys. B*, 1997, **11**, 1067.
- [13] L. Bonnet and J. C. Rayez, *Chem. Phys. Lett.*, 1997, **227**, 183.
- [14] L. Bañares, F. J. Aoiz, P. Honvault, B. Bussery-Honvault, and J. M. Launay, *J. Chem. Phys.*, 2003, **118**, 565.
- [15] L. Bonnet and J. C. Rayez, *Chem. Phys. Lett.*, 2004, **397**, 106.
- [16] T. Xie, J. Bowman, J. W. Duff, M. Braunstein, and B. Ramachandran, *J. Chem. Phys.*, 2005, **122**, 014301.
- [17] M. L. González-Martínez, L. Bonnet, P. Larrégaray, and J. C. Rayez, *J. Chem. Phys.*, 2007, **126**, 041102.
- [18] L. Bonnet, *J. Chem. Phys.*, 2008, **128**, 044109.
- [19] M. L. González-Martínez, W. Arbelo-González, J. Rubayo-Soneira, L. Bonnet, and J. C. Rayez, *Chem. Phys. Lett.*, 2008, **463**, 65.
- [20] W. H. Miller, *Adv. Chem. Phys.*, 1974, **25**, 69.
- [21] J. R. Stine and R. A. Marcus, *Chem. Phys. Lett.*, 1974, **29**, 575.
- [22] M. S. Child, *Semiclassical Mechanics with Molecular Applications*, Oxford, 1991.
- [23] F. J. Aoiz, T. González-Lezana, and V. Sáez-Rábanos, *J. Chem. Phys.*, 2008, **129**, 094305.
- [24] D. M. Wardlaw and R. A. Marcus, *J. Chem. Phys.*, 1985, **83**, 3462.
- [25] E. T. Whittaker, *Treatise on the Analytical Dynamics*, Cambridge University Press, Cambridge, 1989.
- [26] W. H. Miller, *J. Chem. Phys.*, 1971, **54**, 5386.
- [27] I.-C. Chen, J. W. H. Green, and C. B. Moore, *J. Chem. Phys.*, 1988, **89**, 314.
- [28] S. J. Klippenstein and R. A. Marcus, *J. Chem. Phys.*, 1989, **91**, 2280.
- [29] I. Garcia-Moreno, E. R. Lovejoy, and C. B. Moore, *J. Chem. Phys.*, 1994, **100**, 8890.
- [30] S. J. Klippenstein, A. L. L. East, and W. D. Allen, *J. Chem. Phys.*, 1996, **105**, 118.
- [31] K. M. Forsythe, S. K. Gray, S. J. Klippenstein, and G. E. Hall, *J. Chem. Phys.*, 2001, **115**, 2134.
- [32] A. V. Komissarov, M. P. Minitti, A. G. Suits, and G. E. Hall, *J. Chem. Phys.*, 2006, **124**, 014303.
- [33] I. Hamilton and P. Brumer, *J. Chem. Phys.*, 1985, **82**, 595.
- [34] While the same letters are used as for the general Cartesian coordinates, the subscripts in the latter will avoid any confusion.